A palette of bright and photostable monomeric fluorescent proteins for bacterial time-lapse imaging

Nathan Fraikin[1*], Agathe Couturier[1] & Christian Lesterlin[1*]

Molecular Microbiology and Structural Biochemistry (MMSB), Université Lyon 1, CNRS, Inserm, UMR5086, 69007, Lyon, France

*Corresponding authors: Christian.Lesterlin@ibcp.fr ; Nathan.Fraikin@ibcp.fr

Abstract

We report the engineering of novel cyan, green, yellow, and red fluorescent proteins that exhibit improved photostability and aggregation properties while retaining high *in vivo* brightness. Using site-directed mutagenesis in *Escherichia coli*, we first derived the superfolder green fluorescent protein (sfGFP) into mChartreuse, a brighter, more photostable, and monomeric fluorophore. This mChartreuse variant was further derived into cyan and yellow variants with enhanced photostability and dispersibility. We also report a mutation that eliminates residual oligomerization in red fluorescent proteins derived from *Discosoma sp*, such as mCherry or mApple. Incorporation of this mutation in mApple among other substitutions yielded mLychee, a bright and photostable monomeric red fluorescent protein. These novel fluorescent proteins outperform current standards and are, therefore, highly desirable for fluorescence time-lapse analysis in bacteria.

Introduction

Fluorescent proteins (FPs) are crucial tools in life science, enabling the tracking of protein localization and gene expression at the single-cell level (Chudakov et al., 2010). The green fluorescent protein (GFP) was initially cloned from the jellyfish *Aequorea victoria* and initiated a revolution in the study of protein

localization (Chalfie et al., 1994). However, wild-type *A. victoria* GFP (avGFP) showed several shortcomings since it matured poorly at 37°C and required the use of phototoxic ultraviolet light (400 nm) to be excited (Ogawa et al., 1995). Mutagenesis of GFP enabled the discovery of well-folded variants that were excited by blue light (488 nm), such as EGFP, GFPmut2, or superfolder GFP (sfGFP) (Cormack et al., 1996; Pédelacq et al., 2006; Zhang et al., 1996). avGFP derivates also displayed a tendency to dimerize and cause mis-localization of fusion partners, which could be eliminated by disrupting a small hydrophobic dimerization interface with the A206K substitution (Zacharias et al., 2002). Substitution of residues critical for fluorescence also enabled the engineering of blue, cyan, and yellow variants of GFP, expanding the palette of usable FPs (Heim et al., 1994; Ormö et al., 1996). The discovery of a red fluorescent protein (RFP) in *Discosoma sp.* paved the way for multicolor analysis. Indeed, this DsRed protein was homologous to avGFP but excited by yellow light (558 nm), which therefore enabled simultaneous imaging of GFP and DsRed with minimal spectral overlap (Matz et al., 1999). However, engineering usable derivatives of DsRed was extremely challenging since this red FP matures slowly, oligomerizes as a tight tetramer, and can stochastically mature as a green side-product that overlaps with the spectral properties of GFP (Bevis and Glick, 2002). Bevis & Glick overcame the slow maturation of DsRed by random mutagenesis, yielding DsRed-Express, which matured 15 times faster than DsRed (Bevis and Glick, 2002). A *tour-de-force* study by the Tsien lab reported the monomerization of DsRed-Express into a fast-maturing monomeric RFP (mRFP1) through structure-guided disruption of its AB and AC tetramerization interfaces (Campbell et al., 2002). While mRFP1 was dim and bleached quickly when excited, subsequent studies evolved a palette of DsRed derivatives with a wide range of properties, which were called mFruits (Shaner et al., 2008, 2004). Of all mFruits, mCherry became the standard RFP due to its fast maturation, high photostability, and lack of GFP-like side product (Shaner et al., 2004).

Over the years, potentially useful fluorescent proteins were identified in other organisms. For example, an extremely bright yellow FP was identified in the cephalochordate *Branchiostoma lanceolatum* and engineered in a monomeric green FP called mNeonGreen (mNG) (Shaner et al., 2013). mNeonGreen

was twice as bright as EGFP, with similar photostability and maturation kinetics as the latter (Shaner et al., 2013), thereby highlighting the potential for bright and exploitable FPs to be discovered in organisms beyond *A. victoria* and *Discosoma*. Other recently released FPs such as AausFP1 from *Aequorea australis*, mStayGold from *Cyteais uchidae,* or AzaleaB5 from *Montipora monasteriata* show great promise as bright fluorescent probes (Ando et al., 2023b, 2023a; Lambert et al., 2020). Novel FPs could also be engineered *de novo* from a synthetic template as was the case for the mScarlet family (Bindels et al., 2016). Further evolution of mScarlet yielded mScarlet3 and mScarlet-I3, the brightest red FPs to date (Gadella et al., 2023).

All FPs have different sets of parameters that dictate setups for which they should be used. These include fluorescence spectrum, brightness, maturation rate, photostability and dispersibility (Cranfill et al., 2016). Brightness of FPs is measured as the product of its extinction coefficient and quantum yield and represents the amount of signal that can be obtained from a given FP. However, another critical parameter that influences *in vivo* brightness is maturation rate, which defines the kinetics by which a folded dark FP is converted into a fluorescent species by cyclization of three amino acids that become its chromophore. Because bacteria tend to be fast-growing organisms, the use of fast-maturing FPs is of utmost importance in these organisms to achieve high brightness, since dark species of slow-maturing FPs would quickly get diluted by fast doublings (Balleza et al., 2018).

Here, we used site-directed mutagenesis to engineer high-performance fluorescent proteins. We report the development of four new FP that offer superior brightness and photostability while being truly monomeric. We developed mChartreuse from sfGFP by introducing 6 mutations (N39I, I128S, D129G, F145Y, N149K & V206K) that enhanced brightness, photostability, and monomericity (**Figure 1**). We further developed mChartreuse into mJuniper, a cyan variant, with the addition of four mutations (Y66W, S72A, N146F & H148D), and into mLemon, a yellow variant, with the addition of five mutations (T63S, T65G, S72A, T203Y & V224L) (**Figure 1**). Compared to state-of-the-art cyan and yellow FPs, these two FP offer superior dispersibility and photostability with similar brightness.

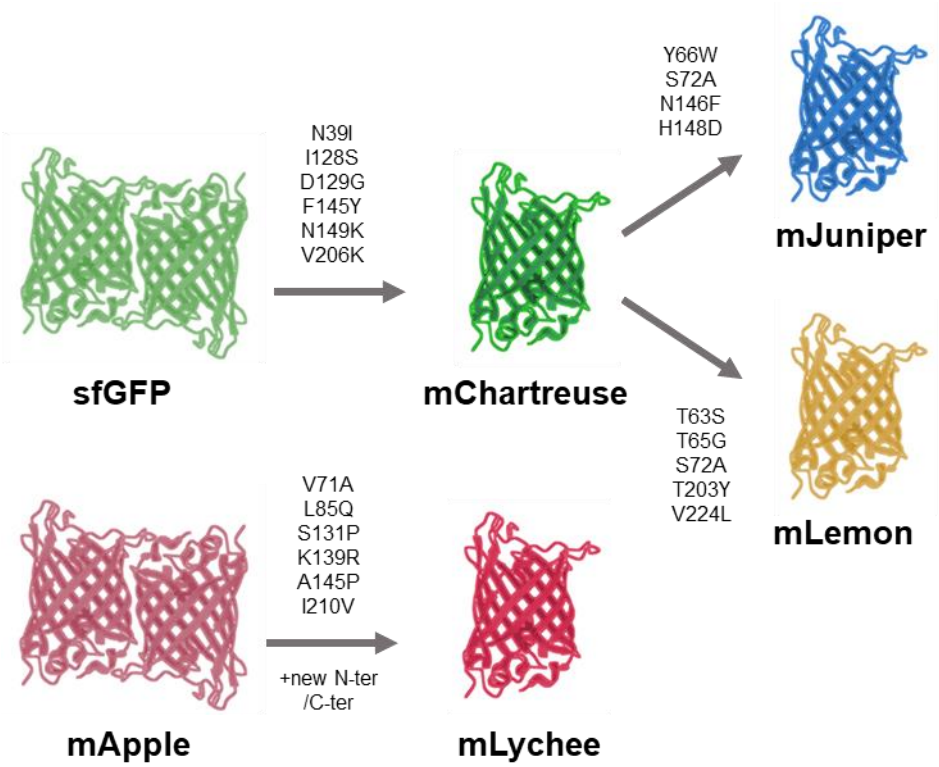

Figure 1: Flow chart of fluorescent proteins developed in this study. Each arrow shows a development step with its associated substitutions. New N-ter/C-ter refers to the replacement of mApple N and C-termini with those of mCherry2C (Valbuena et al., 2020).

While engineering red FPs, we identified S131P, a substitution that eliminates oligomerization of supposedly monomeric DsRed derivatives in *E. coli*. By combining S131P with brightness-enhancing mutations (V71A, L85Q, K139R, A145P & I210V), we evolved mApple into mLychee, a bright, monomeric and photostable red FP (**Figure 1**). We therefore offer a palette of novel high-performance fluorescent proteins tested in *E. coli*, developed by microbiologists for microbiologists.

Results

Site-directed mutagenesis improves all properties of sfGFP

We first aimed to obtain an improved GFP derived from the well characterized *A. victoria* GFP (avGFP) ancestor protein. We chose sfGFP as a starting template due to its improved folding, fast maturation,

high brightness, and broad use in bacterial models (Balleza et al., 2018; Pédelacq et al., 2006). We first introduced the V206K monomerizing mutation and the F145Y photostability-improving mutation as previously described for the construction of msGFP2 (Valbuena et al., 2020). To further improve the brightness of this starting template, we used high-throughput flow cytometry to screen several mutations found in bright GFP homologs. After four rounds of site-directed mutagenesis, we identified our brightest variant containing mutations N39I, I128S, D129G from the Achilles YFP (Yoshioka-Kobayashi et al., 2020) and N149K from the Emerald GFP (Teerawanichpan et al., 2007) (**Figure 2A, Supplementary Figure 1**). We called this variant mChartreuse in reference to the similarly colored liquor from southeast France. By fusing mChartreuse and other GFPs with mCherry, we can evaluate the *in vivo* brightness of these FPs in growing cells followed by normalizing the green fluorescence signal to that of mCherry, therefore allowing us to compensate for any potential variation in the expression level of these constructs (Bindels et al., 2016) (**Figure 2B**). Our results show that mChartreuse is 30% brighter than sfGFP in *E. coli* (**Figure 2C**). mChartreuse is also brighter than mNeonGreen and mGreenLantern, two bright and top-performing GFPs that will be used hereafter as comparison points to sfGFP and mChartreuse (Campbell et al., 2020; Shaner et al., 2013) (**Figure 2C**).

To easily assess how well mChartreuse matured in exponentially growing *E. coli*, we quantified the maturation extent of mChartreuse and other green FPs by shutting down translation using tetracycline, and by measuring fluorescence before and after 3 h of tetracycline treatment (**Figure 2D**). In this setup, tetracycline arrests protein synthesis, allowing remaining dark unmatured fluorophores to fully mature. All tested green FPs displayed maturation ratios in the same range, between 0.73 and 0.82 (**Figure 2E**), suggesting that these four FPs display similar maturation rates and kinetics.

The excitation and emission spectra of mChartreuse were determined from crude cell extracts where this FP was expressed. Our mChartreuse displays a broad excitation peak with a maximum at 488 nm and a shoulder at 470 nm, while its emission peaked at 511 nm, similar to that of superfolder GFP or EGFP (Pédelacq et al., 2006; Zhang et al., 1996) (**Figure 2F**).

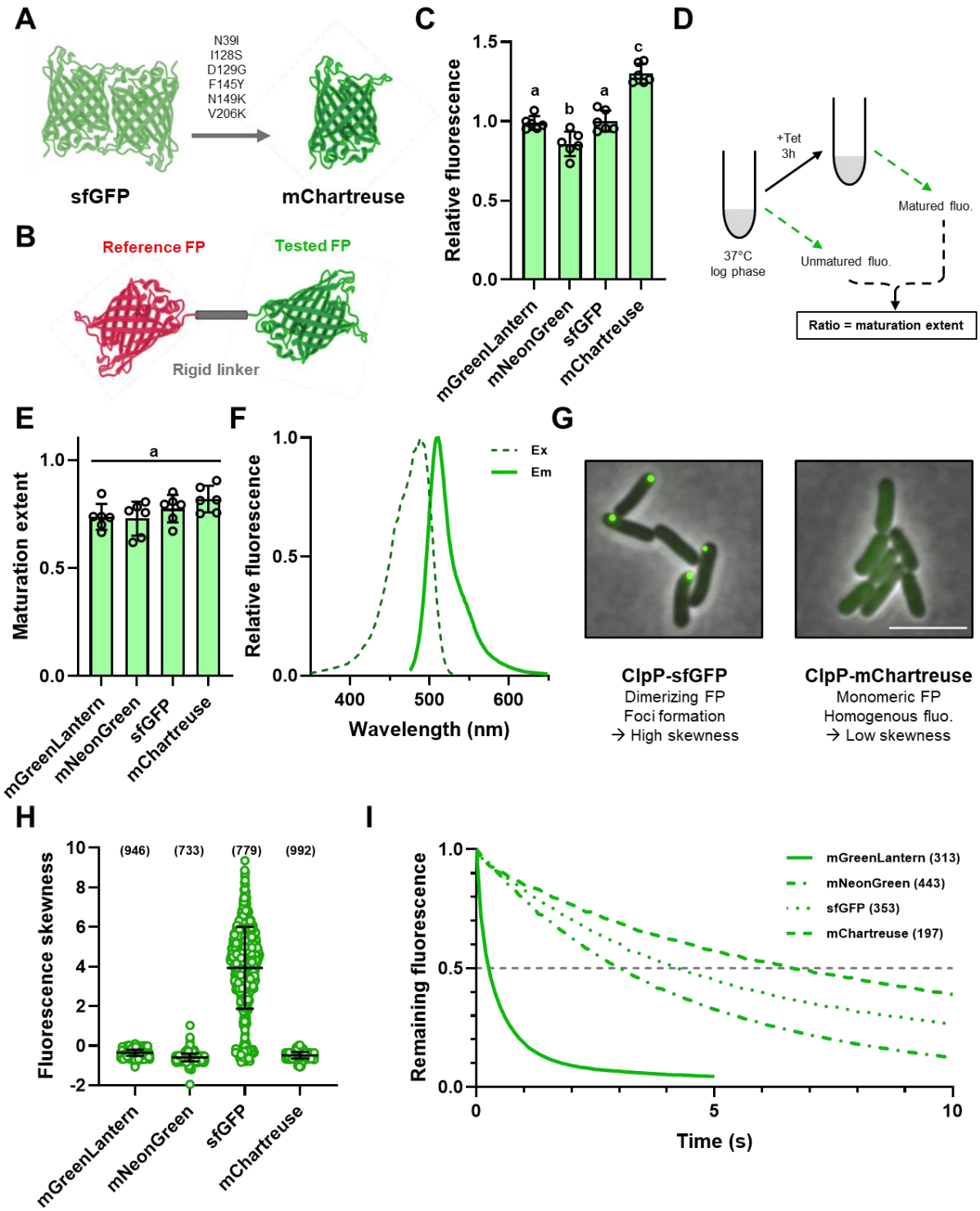

Figure 2: Development and characterization of the mChartreuse green fluorescent protein. A : All six mutations introduced in sfGFP to obtain mChartreuse. **B:** Representation of the brightness quantification system developed by (Bindels et al., 2016), where the tested FP is fused to a spectrally distinct FP. The ratiometric measurement of the tested FP normalized to that of the reference FP enables to offset any variation in FP signal due to differences in expression levels. The rigid spatial linker that separates both FPs prevents fluorescence resonance energy transfer (FRET). **C:** *In vivo* brightness quantification of green FPs. Green FP fluorescence was measured in exponentially growing cultures and normalized to that of mCherry. Data shows mean and standard deviation of six independent replicates. Letters show groups of datasets with no statistically significant differences (ANOVA & Bonferroni post-hoc, p>0.05). **D:** Description of the maturation assay. Exponentially growing cells were treated with 15 µg/ml tetracycline hydrochloride to inhibit translation and enable full maturation of dark unmatured fluorophores. Fluorescence was measured before and 3 hours after tetracycline addition, with the ratio between these two measures yielding an estimation of the maturation extent of the fluorophore. Letters show groups of datasets with no

statistically significant differences (ANOVA & Bonferroni post-hoc, p>0.05). **E:** Maturation extents of green FPs 3 hours before and after tetracycline addition. Data shows mean and standard deviation of six independent replicates. **F:** Fluorescence spectrum of mChartreuse. The dashed line shows the excitation spectrum (fixed emission at 555 nm) and the full line shows the emission spectrum (fixed 450 nm excitation). Data is shown as the mean of two spectrum acquisitions. **G:** Representative images of ClpP fusions. Fusion of ClpP with a dimeric FP (*i.e.* sfGFP) causes substantial aggregation, which leads to the formation of fluorescence foci and high fluorescence skewness in single cells. Fusion with a monomeric FP (*i.e.* mChartreuse) does not cause aggregation, leading to homogenous FP distribution in the cytosol and low fluorescence skewness. **H:** Fluorescence distribution skewness of single cells expressing ClpP-FP fusions. Bars show the mean and standard deviation. Data were acquired from three independent experiments, with the total numbers of analyzed bacteria shown in brackets. **I:** Photostability of FP signals in live bacteria illuminated with 100 ms steps and normalized to intensity at time 0. The dashed grey line shows the cutoff at which $t_{1/2}$ were calculated. Data were acquired from three independent experiments, with the total numbers of analyzed bacteria shown in brackets.

We evaluated the dispersibility and oligomerization of mChartreuse and other green FPs by fusing them to the ClpP protease as previously described (Landgraf et al., 2012). In this system, oligomeric FPs cause cooperative clustering of ClpP homo-tetradecamers into fluorescent foci, while monomeric FPs do not perturbate the homogenous cytosolic localization of ClpP (Landgraf et al., 2012). To offer an unbiased quantification of foci formation by these ClpP fusions, we measured the skewness of pixel intensity distributions in single bacteria as a proxy for fluorescence heterogeneity within cells (Ducret et al., 2016). As previously described, fusion of ClpP with sfGFP (a dimerizing FP) induced foci formation, relfected by the high fluorescence skewness observed (**Figure 2G-H**). On the other hand, ClpP fusions with mChartreuse, mNeonGreen and mGreenLantern all displayed homogeneous fluorescence as shown by the low fluorescence skewness values of these fusions (**Figure 2G-H**). Our results therefore show that mChartreuse is monomeric in *E. coli*.

Because photostability is a critical parameter for time-lapse imaging, we evaluated the time required to bleach mChartreuse to half its original fluorescence intensity ($t_{1/2}$) by time-lapse fluorescence microscopy. Of tested GFPs, mChartreuse displayed the highest photostability ($t_{1/2}$ = 6.7 s), followed by sfGFP ($t_{1/2}$ = 4.3 s), mNeonGreen ($t_{1/2}$ = 3.0 s), and finally mGreenLantern ($t_{1/2}$ = 0.3 s) (**Figure 2I**). Altogether, our results show that our mChartreuse improved the brightness, dispersibility, and photostability of sfGFP, making it a superior choice for all applications.

Site-directed mutagenesis of mChartreuse yields highly photostable monomeric cyan and yellow FPs.

Since mChartreuse is a bright and photostable variant of sfGFP, we assessed whether this FP could be derived into cyan and yellow variants with superior properties. We developed a cyan variant of mChartreuse by introducing the Y66W cyan-determining mutation (Heim et al., 1994), followed by the S72A, N146F, and H148D mutations that are responsible for the high brightness of mTurquoise2 (Goedhart et al., 2012) (**Figure 3A, Supplementary Figure 1**). This variant, named "mJuniper", was compared to SCFP3A and mTurquoise2, two top-performing CFPs (Goedhart et al., 2012; Kremers et al., 2006). The brightness of mCherry-fused mJuniper was equivalent to that of SCFP3A, with both these FPs being roughly 50% brighter than mTurquoise2 (**Figure 3B**). mJuniper also displayed high maturation extent (0.93) in growing cells compared to SCFP3A (0.71) and mTurquoise2 (0.34) (**Figure 3C**). mJuniper showed two excitation peaks at 436 and 455 nm, and two emission peaks at 475 and 504 nm, as described for SCFP3A and mTurquoise2 (Goedhart et al., 2012; Kremers et al., 2006) (**Figure 3D**). Fusions of ClpP with mTurquoise2 and SCFP3A both lead to foci formation in a significant number of cells while fusion of ClpP with mJuniper yielded homogenous fluorescence, showing that mJuniper is truly monomeric in *E. coli* cells (**Figure 3E**). Moreover, mJuniper displayed higher photostability ($t_{1/2}$ = 2.2 s) compared to mTurquoise2 ($t_{1/2}$ = 1.1 s) and SCFP3A ($t_{1/2}$ = 1.1 s) (**Figure 3F**). Therefore, mJuniper is a bright and monomeric cyan FP with superior maturation and photostability in *E. coli*.

A yellow variant of mChartreuse was engineered by first introducing the T656, S72A and T203Y yellow-determining mutation that were first introduced in the enhanced yellow FP (EYFP) (Ormö et al., 1996) (**Figure 3A, Supplementary Figure 1**). We also added the T63S mutation from mGold and the V224L from YPet to enhance photostability (Lee et al., 2020; Nguyen and Daugherty, 2005) (**Figure 3A**). We called this variant "mLemon" and compared it to mYPet (YPet A206K) and SYFP2 (mVenus L68V), two top-performing YFPs (Kremers et al., 2006; Nguyen and Daugherty, 2005). SYFP2 and mLemon were both brighter than mYPet, with mLemon showing 90% of the brightness of SYFP2 (**Figure 3B**). Similarly to brightness, the maturation extent of mLemon (0.65) was between that of SYFP2 (0.76) and

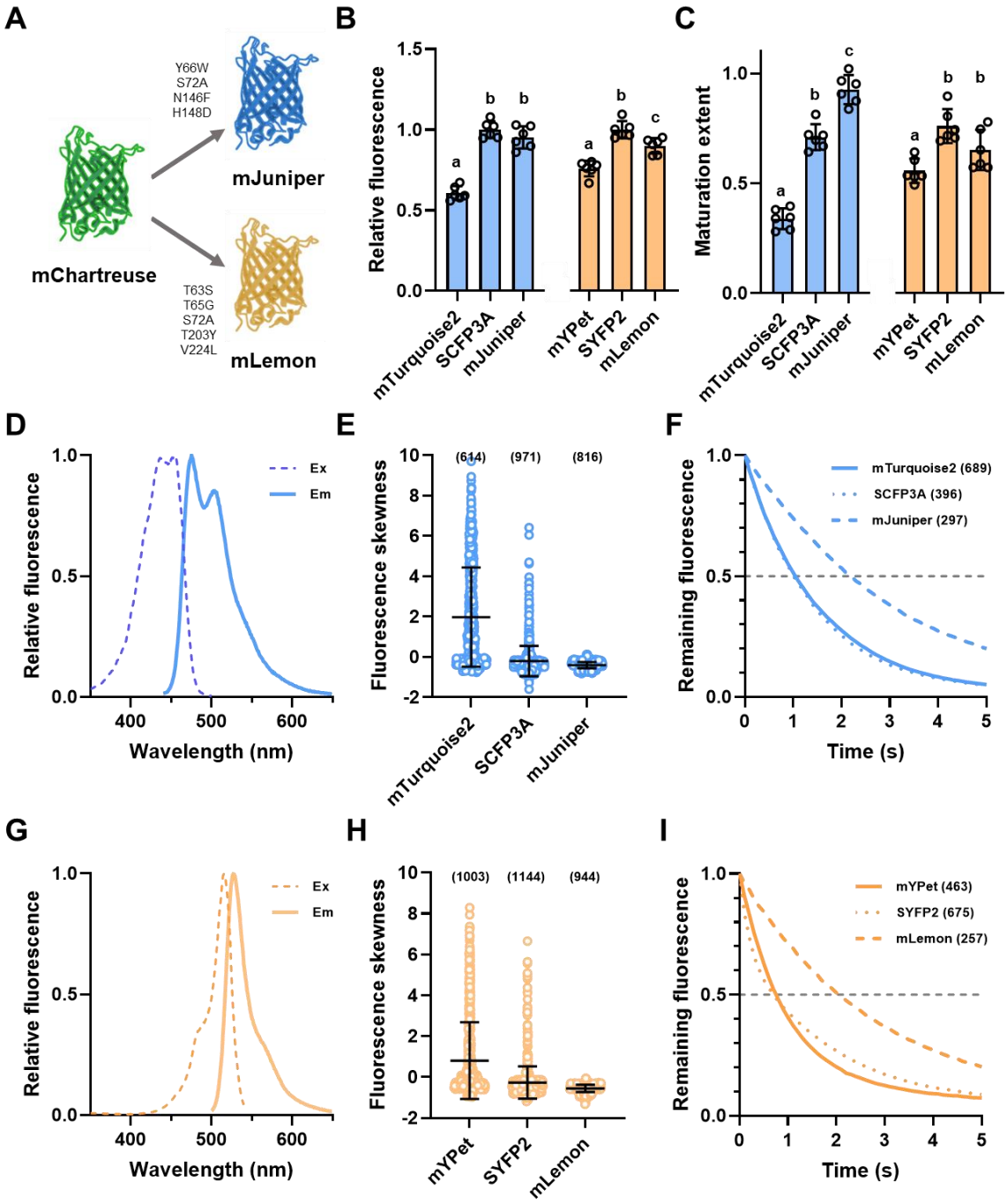

Figure 3: Development and characterization of cyan and yellow variants of mChartreuse. A: Mutations introduced in mChartreuse to obtain the mJuniper cyan variant and the mLemon yellow variant. **B:** *In vivo* brightness quantification of cyan and yellow FPs. Fluorescence was measured in exponentially growing cultures and normalized to that of mCherry (for cyan FPs) or mTurquoise2 (for yellow FPs). Data shows mean and standard deviation of six independent replicates. Letters show groups of datasets with no statistically significant differences (ANOVA & Bonferroni post-hoc, p>0.05). **C:** Maturation extents of cyan and yellow FPs 3 hours before and after addition of 15 µg/ml tetracycline hydrochloride. Data shows mean and standard deviation of six independent replicates. Letters show groups of datasets with no statistically significant differences (ANOVA & Bonferroni post-hoc, p>0.05). **D & G:** Fluorescence spectra of mJuniper (**D**) and mLemon (**G**). The dashed line shows excitation spectra (fixed 530 nm emission for mJuniper and 570 nm for mLemon) and the full line shows the emission spectrum (fixed 410 nm excitation for mJuniper and 470 nm for mLemon). Data is shown as the mean of two spectrum acquisitions. **E & H:** Fluorescence distribution skewness of single cells expressing ClpP-CFP (**E**) or ClpP-YFP (**H**) fusions. Bars show the mean and standard deviation. Data were acquired from three independent experiments, with the total numbers of analyzed bacteria shown in brackets. **F & I:** Photostability of CFP signals (**F**) and YFP signals (**I**) in live bacteria illuminated with 100 ms steps and normalized to intensity at time 0. The dashed grey line shows the cutoff at which $t_{1/2}$ were calculated. Data were acquired from three independent experiments, with the total numbers of analyzed bacteria shown in brackets.

mYPet (0.56), suggesting that differences in apparent brightness in these FPs are mainly due to differences in maturation (**Figure 3C**). The spectrum of mLemon was similar to that of other yellow FPs (Kremers et al., 2006; Nguyen and Daugherty, 2005), with narrow excitation and emission peaks at 516 and 528 nm, respectively (**Figure 3G**). ClpP-mLemon displayed homogenous fluorescence while ClpP-mYPet and ClpP-SYFP2 both showed aggregation, showing that mLemon is monomeric (**Figure 3H**). mLemon displayed more than twice the photostability ($t_{1/2}$ = 2.1 s) of mYPet ($t_{1/2}$ = 0.8 s) and SYFP2 ($t_{1/2}$ = 0.8 s) (**Figure 3I**). Therefore, mLemon offers higher photostability and lower aggregation compared to other yellow FPs while still retaining high brightness.

Monomerization and enhancement of the mApple red FP.

We also sought to engineer a bright and photostable monomeric red fluorescent protein. While mScarlet-I3 was monomeric and offered unrivaled brightness, it showed lower photostability compared to other red FPs (Gadella et al., 2023). On the other hand, mFruits like mCherry and mApple offered higher photostability (Shaner et al., 2008, 2004). However, previous data shows that mFruits aggregate when fused to ClpP in *E. coli* (Landgraf et al., 2012). Indeed, our skewness analysis shows that fusions of mCherry and mApple with ClpP had a high propensity to form foci, confirming that these FPs are not monomeric in *E. coli* (**Figure 4A**). On the other hand, ClpP-mScarlet-I3 did not form foci and behaves as a truly monomeric FP (**Figure 4A**). Since mScarlet-I3 was derived from a mFruit-based synthetic template, we introduced mutations specific to mScarlet-I3 into mApple, then screened for mutations conferring a non-aggregative behavior in ClpP fusions. The S131P mutation (numbering relative to DsRed) abolished foci formation in ClpP fusions with mApple or mCherry (**Figure 4A**). In DsRed tetramers, S131 is part of the AB tetramer interface between two DsRed protomers, with the hydroxyl sidechain and the amide nitrogen of S131 each implicated in a hydrogen bond with the carboxyl sidechain of D154 located *in trans* (**Figure 4B**). Therefore, it is likely that the substitution of S131 with a proline would prevent H-bond formation with D154 and eliminates residual dimerization of mFruits in *E. coli*.

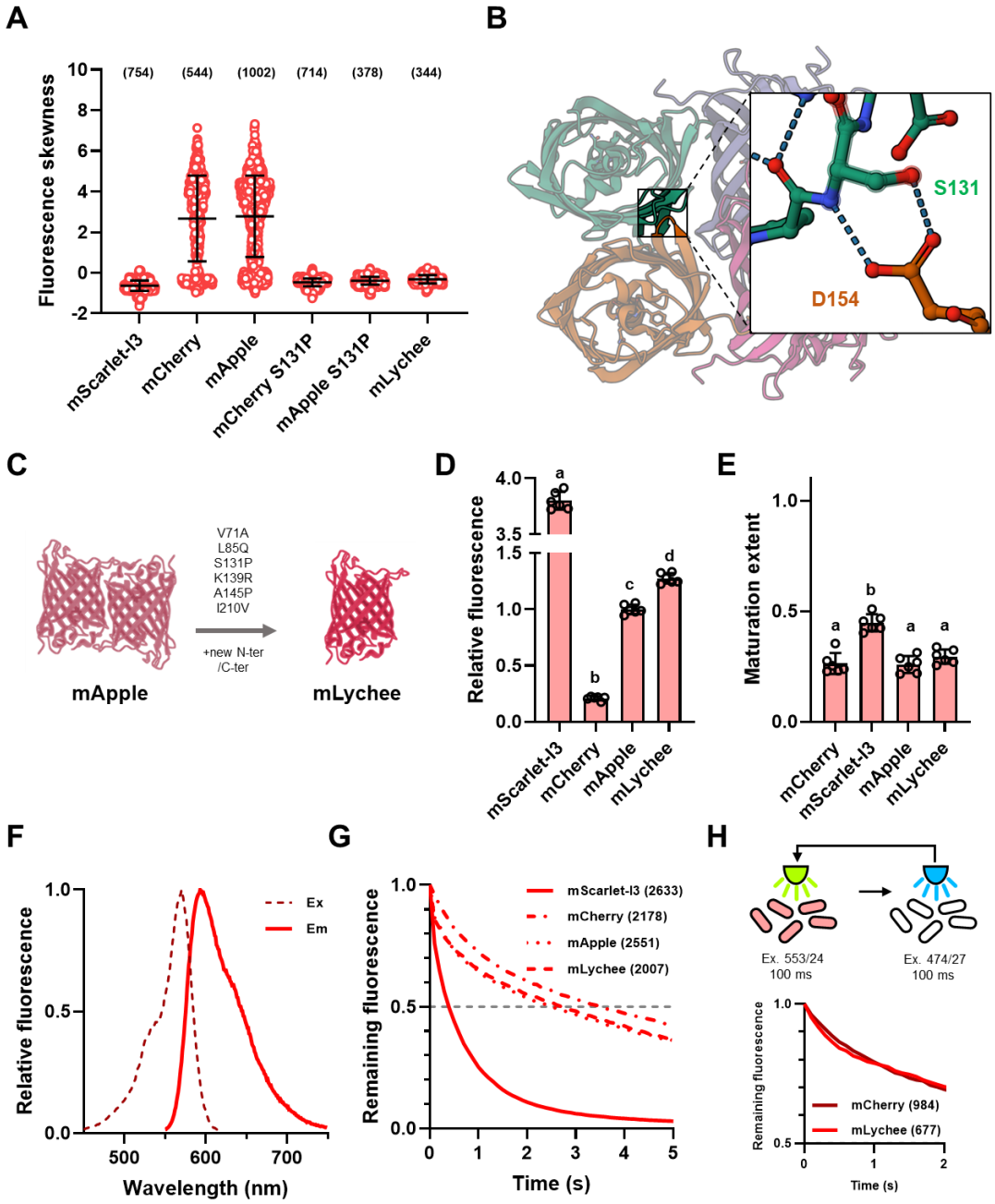

Figure 4: Development and characterization of the mLychee red fluorescent protein. A: Fluorescence distribution skewness of single cells expressing ClpP-FP fusions. Bars show the mean and standard deviation. Data were acquired from three independent experiments, with the total numbers of analyzed bacteria shown in brackets. **B:** Location of serine 131 (S131) in the AB dimerization interface of a DsRed tetramer (PDB 1ZGO) shown in ribbon representation. The inlet shows the interaction between S131 and aspartate 154 (D154) located *in trans* at the atomic level, with putative hydrogen bonds shown as dashed lines. **C:** All six mutations introduced in mApple to obtain mLychee. **D:** *In vivo* brightness quantification of red FPs. Fluorescence was measured in exponentially growing cultures and normalized to that mTurquoise2. Data shows mean and standard deviation of six independent replicates. Letters show groups of datasets with no statistically significant differences (ANOVA & Bonferroni post-hoc, p>0.05). **E:** Maturation extents of red FPs 3 hours before and after addition of 15 µg/ml tetracycline hydrochloride. Data shows mean and standard deviation of six independent replicates. Letters show groups of datasets with no statistically significant differences (ANOVA & Bonferroni post-hoc, p>0.05). **F:** Fluorescence spectrum of mLychee. The dashed line shows excitation spectra (fixed 640 nm emission) and the full line shows the emission spectrum (fixed 525 nm excitation). Data is shown as the mean of two spectrum acquisitions. **G:** Photostability of FP signals in live bacteria illuminated with 100 ms steps and normalized to intensity at time 0. The dashed grey line shows the cutoff at which $t_{1/2}$ were calculated. Data were acquired from three independent experiments, with the total numbers of analyzed bacteria shown in brackets. **H:** Short-term photostability of mCherry and mLychee signals under alternating green (553 nm) and blue (474 nm) illumination. Data from three independent experiments, total numbers of analyzed bacteria shown in brackets.

Due to the superior brightness of mApple, we used mApple-S131P as a starting template to engineer a brighter RFP. During the previous engineering of mFruits, the original N and C-termini of DsRed were replaced with those of avGFP (Shaner et al., 2004). While this allowed proper localization of some fusions, restoration of DsRed-like termini was shown to improve brightness and relieve RFP-induced cytotoxicity (Gadella et al., 2023; Valbuena et al., 2020). We therefore synthetized a codon-optimized mApple template, replaced the MVSKGEENNM N-terminus and TGGMDE C-terminus of mApple with the MDSTE N-terminus and GSQGGSGGS C-terminus of mCherry2C (Valbuena et al., 2020). We subsequently performed rounds of site-directed mutagenesis to identify mutations conferring increased *in vivo* brightness. Mutations V71A, L85Q, K139R, A145P, and I210V were incorporated in our final variant, baptized mLychee (**Figure 4C, Supplementary Figure 2**).

While mScarlet-I3 is more than three times brighter than mApple, mLychee is 28% brighter than mApple, and six times brighter than mCherry under excitation at 565 nm (**Figure 4D**). mCherry, mApple, and mLychee showed maturation ratios in the same range (0.26-0.30) while mScarlet-I3 showed better maturation (0.45) (**Figure 4E**). Similarly to what was published for mScarlets and mApple (Bindels et al., 2016; Gadella et al., 2023; Shaner et al., 2008), mLychee shows a single excitation peak at 570 nm and an emission peak at 593 nm (**Figure 5F**). mCherry displayed the highest photostability ($t_{1/2}$ = 3.6 s) while mScarlet-I3 bleached the quickest ($t_{1/2}$ = 0.4 s) (**Figure 5G**). mApple and mLychee displayed complex bleaching behaviors, with an abrupt loss of 15% of their signal after the first 100 ms exposure, followed by slow bleaching kinetics similar to that of mCherry ($t_{1/2}$ = 2.7 s & 2.8 s, respectively) (**Figure 5G**). Previous results showed that this fast initial bleaching of mApple was a photochromic phenomenon reversible either by time or by illuminating this fluorophore with blue light (Shaner et al., 2008). We therefore quantified the bleaching of mLychee by alternating illuminations between 553 and 474 nm (**Figure 5H**). In these conditions, the fast initial bleaching of mLychee was practically eliminated, yielding initial bleaching kinetics similar to that of mCherry (**Figure 5H**). Therefore, mLychee is a truly monomeric red FP that offers an excellent balance between brightness and photostability.

Discussion

In this manuscript, we have described a palette of novel bright, monomeric, and photostable fluorescent proteins for use in bacteria. Our four FPs, mChartreuse (green), mJuniper (cyan), mLemon (yellow), and mLychee (red), all offer high brightness, robust photostability, and low aggregation, making them very desirable fusion tags for time-lapse imaging. Contrasting with other bright modern FPs like mNeonGreen or StayGold, mChartreuse, and its derivatives were evolved from sfGFP, a well-folded green FP that is well described and broadly used by molecular microbiologists. Constructs that currently use sfGFP can therefore be quickly adapted to use mChartreuse, mJuniper, and mLemon using identical primers. Our novel fluorophores also share their spectral properties with current standards, which can therefore be imaged with standard optical configurations and filters.

Strikingly, we observed that state-of-the-art monomeric cyan, yellow and red FPs tend to aggregate when fused to ClpP, as previously shown for mVenus, mYPet and mCherry (Landgraf et al., 2012). By contrast, mJuniper, mLemon and mLychee do not aggregate when fused to ClpP. While the reasons for these discrepancies have not been investigated, we believe that superfolder mutations present in our original sfGFP template (S30R, F99S, N105T & I171V) could be beneficial in preventing aggregation. We have also established a quantitative metric to measure FP aggregation in *E. coli* based on ClpP fusions (Landgraf et al., 2012). Computing the skewness in fluorescence distribution of single bacteria can be used as an unbiased descriptor of fluorescence homogeneity that does not rely on human or threshold-based detection of foci, therefore enabling reproducible quantification of FP aggregation and fluorescent foci formation.

Previous research showed that mCherry and mApple are monomers in mammalian cells when assayed using the Organized Smooth Endoplasmic Reticulum (OSER) approach (Bindels et al., 2016; Cranfill et al., 2016). However, fusions of mCherry with ClpP, IbpA or RpoS in *E. coli* all caused substantial aggregation (Goormaghtigh et al., 2018; Govers et al., 2018; Landgraf et al., 2012), suggesting that mFruits are not monomeric in bacterial cells. The reasons for these discrepancies are not known but

might stem from the differences in cytosolic composition and crowding between mammalian and bacterial cells. Because some fluorophores appear monomeric in some models but aggregate in others, their transferability between different model organisms should be investigated on a case-by-case basis. Nevertheless, we have identified serine 131 of mFruits as responsible for these aggregating properties, which could be eliminated by substituting this residue for a proline. This mutation was incorporated in our mLychee variant developed from mApple. While mLychee is dimmer than mScarlet-I3, it compensates for this lack of brightness with robust photostability. Our mLychee would therefore be suited for time-lapse imaging while mScarlet-I3 would remain preferable for endpoint methods where bleaching is less of an issue (*e.g.* microscopy snapshots, flow cytometry). Even though mScarlet-I3 is brighter than mLychee, both proteins are based on the same DsRed scaffold and display more than 80% identity at the amino acid sequence level, suggesting that there is room to improve the brightness and maturation of mLychee. Further testing of these novel fluorescent proteins as fusion tags in *E. coli* and other bacterial species will enable us to assess how well such fusions preserve native localization and activities of essential prokaryotic proteins.

Methods

Molecular cloning

All plasmid constructs were obtained by Gibson assembly unless specified otherwise and are detailed in **Table S1**. All primers used to construct these vectors are detailed in **Table S2**. All enzymes were purchased from New England Biolabs. Polymerase chain reactions were performed using PrimeSTAR Max (Takara). Synthetic genes for mGreenLantern and mLychee were ordered from Integrated DNA Technologies.

pNF02 vectors used for unfused FP expression were constructed by amplifying a mini-F backbone from pNF02-mScarlet-I (Goormaghtigh et al., 2018) using primers bbpNF02 F & R. mChartreuse, mJuniper, and mLemon were amplified using primers sfGFP02 F & R while mLychee was directly inserted as a synthetic gene. pFN01 vectors, which encode all tested FPs fused to a reference FP and separated with

a rigid linker, were constructed by amplifying a mTurquoise2-linker-mScarlet-I3 fragment from pDress-mTq2-link-mSc-I3 (Gadella et al., 2023) with primers IpFN01 F & R and a mini-F backbone from pNF02 using VpFN01 F & R. Red and yellow FPs were amplified using primer pairs 01miscF & R (mCherry, mApple, SYFP2), 01YPet F & R (mYPet), and 01sfGFP F & R (mLemon) on their respective templates (**Table S1**) (Gadella et al., 2023; Shaner et al., 2008). To clone green and cyan FPs, mTurquoise2 was first replaced by mCherry on pFN01 by amplification of the backbone using VmTq2mCh F & R and by amplification of mCherry from pROD62 using ImTq2mCh F & R. Subsequently, FPs were cloned in this vector using primers 01sfGFP F & R (sfGFP, mChartreuse, mJuniper), 01mNGb F & R (mNeonGreen), mGL F & 01sfGFP R (mGreenLantern), and 01misc F & R (mTurquoise2) amplified from their respective templates (**Table S1**) (Gadella et al., 2023; Rousseau et al., 2023). A pFN01-mCh-SCFP3A was generated by site-directed mutagenesis from pFN01-mCh-mTq2 using VSCFP3A F & R and ISCFP3A F & R.

The pCLP vector used to fuse FPs to ClpP was constructed by amplifying *clpP* and its native promoter using primers clpP F & R. This fragment was digested with NheI and BamHI and cloned in pUA66 (Zaslaver et al., 2006) digested with AvrII and BamHI. To construct ClpP-FP fusions, FPs were amplified from corresponding pFN01 vectors with primers insCLP F & R and cloned in a pCLP backbone amplified with pCLP F & R.

General procedures

E. coli TB28 (MG1655 Δ*lacIZYA*) (Bernhardt and De Boer, 2003) was used in all experiments except those involving ClpP fusions, which were performed in strain LY3581 (MG1655 Δ*clpP::FRT*). Strain LY3581 was constructed by P1 transduction of the *clpP* deletion from strain JW0427 (Baba et al., 2006). All experiments were performed by growing cells in M9 medium (7 g/L $Na_2HPO_4.7H_2O$, 3 g/L KH_2PO_4, 0.5 g/L NaCl, 1 g/L NH_4Cl, 1 mM $MgSO_4$, 80 µM $CaCl_2$) supplemented with 0.2% glucose, 0.4% casamino acids and 0.4 mg/L thiamine hydrochloride (referred to as M9GC). Overnight cultures were inoculated in M9GC containing appropriate antibiotics (10 µg/ml chloramphenicol for pFN01/pNF02 or 25 µg/ml kanamycin for pCLP) from colonies, followed by 1000x dilution in fresh M9GC medium without

antibiotics. Cells were then grown to exponential phase, to a turbidity (OD_{600}) of 0.2-0.3 at which experiments were performed. Fluorescence in bulk cultures was measured in 96 well plates using a Spark plate reader (Tecan). Cyan fluorescence was excited at 450 nm and collected at 480 nm, green fluorescence was excited at 470 nm and collected at 510 nm, yellow fluorescence was excited at 510 nm and collected at 540 nm, and red fluorescence was excited at 565 nm and collected at 595 nm. All measures were performed using a monochromator with a 5 nm bandpass. Fluorescence spectra were determined from crude extract of cells constitutively expressing FPs from pNF02 vectors. Such extracts were prepared by centrifuging 5ml of overnight culture and resuspending it in 500 µl of buffer 1 (50 mM Tris-HCl pH 7.5, 5 mM EDTA & 150 mM NaCl), followed by beating with 250µl of 100 µm glass beads (1400 RPM, 5 min).

Microscopy procedures

Bacteria grown as described in general procedures were sealed on M9GC pads containing 1% agarose using GeneFrames (ThermoFisher). Cells were imaged using an Eclipse Ti2 microscope (Nikon) equipped with a Plan Apo λ 100x/1.45 objective, a motorized stage, Z-drift correction (Perfect Focus System, Nikon), heating (Okolab), a solid-state light source (Spectra X, Lumencor) and a sCMOS camera (Orca-Fusion BT, Hamamatsu). Cyan fluorescence was excited using a 438/24 excitation filter and collected using a 482/25 emission filter, green fluorescence was excited using a 474/27 excitation filter and a 515/30 emission filter, yellow fluorescence was excited using a 509/22 excitation filter and a 544/25 emission filter. Red fluorescent proteins were excited using a 578/21 excitation filter and a 641/75 emission filter for ClpP fusions or with a 553/24 excitation filter for photostability experiments. All fluorescent proteins were imaged using *ad-hoc* LEDs at 50% power intensity with 100 ms exposure times, except RFP photostability experiments which used 12% power of the 555 nm LED. Images were subsequently processed using MicrobeJ by automatic detection of cells and quantification of fluorescence parameters (*i.e.* mean for photostability experiments, skewness for ClpP fusions) (Ducret et al., 2016). Photobleaching experiments were performed by bleaching live cells by 100 ms steps with

appropriate excitation settings as described above. Photobleaching half-times were determined as time at which the mean fluorescence of the population dropped below 0.5.

Acknowledgments

N.F. and C.L. conceptualized the paper. N.F. and A.C. performed experiments and analyzed the data. N.F. wrote the paper and prepared the figures, with input from C.L. and A.C.. C.L. provided funding (Foundation for Medical Research, Grant number FRM-EQU202103012587 to C.L. and A.C.; French National Research Agency, Grant number ANR-23-CE12-0037 to C.L and N.F.). Plasmids pDRESS-mTq2-link-mSc-I3 and pDX-mSc3-SYFP2 were kind gifts from T.W.J. Gadella obtained through Addgene (plasmids 189755 & 189764). Plasmids encoding mChartreuse, mJuniper, mLemon and mLychee will be available on Addgene.

References

Ando, R., Sakaue-Sawano, A., Shoda, K., Miyawaki, A., 2023a. Two coral fluorescent proteins of distinct colors for sharp visualization of cell-cycle progression. Cell Structure and Function 48, 135–144. https://doi.org/10.1247/csf.23028

Ando, R., Shimozono, S., Ago, H., Takagi, M., Sugiyama, M., Kurokawa, H., Hirano, M., Niino, Y., Ueno, G., Ishidate, F., Fujiwara, T., Okada, Y., Yamamoto, M., Miyawaki, A., 2023b. StayGold variants for molecular fusion and membrane-targeting applications. Nature Methods. https://doi.org/10.1038/s41592-023-02085-6

Baba, T., Ara, T., Hasegawa, M., Takai, Y., Okumura, Y., Baba, M., Datsenko, K.A., Tomita, M., Wanner, B.L., Mori, H., 2006. Construction of Escherichia coli K-12 in-frame, single-gene knockout mutants: the Keio collection. Molecular Systems Biology 2, 2006.0008. https://doi.org/10.1038/msb4100050

Balleza, E., Kim, J.M., Cluzel, P., 2018. Systematic characterization of maturation time of fluorescent proteins in living cells. Nature Methods 15, 47–51. https://doi.org/10.1038/nmeth.4509

Bernhardt, T.G., De Boer, P.A.J., 2003. The Escherichia coli amidase AmiC is a periplasmic septal ring component exported via the twin-arginine transport pathway. Molecular Microbiology 48, 1171–1182. https://doi.org/10.1046/j.1365-2958.2003.03511.x

Bevis, B.J., Glick, B.S., 2002. Rapidly maturing variants of the Discosoma red fluorescent protein (DsRed). Nature Biotechnology 20, 83–87. https://doi.org/10.1038/nbt0102-83

Bindels, D.S., Haarbosch, L., van Weeren, L., Postma, M., Wiese, K.E., Mastop, M., Aumonier, S., Gotthard, G., Royant, A., Hink, M.A., Gadella Jr, T.W.J., 2016. mScarlet: a bright monomeric red fluorescent protein for cellular imaging. Nature Methods 14, 53.

Campbell, B.C., Nabel, E.M., Murdock, M.H., Lao-Peregrin, C., Tsoulfas, P., Blackmore, M.G., Lee, F.S., Liston, C., Morishita, H., Petsko, G.A., 2020. mGreenLantern: a bright monomeric fluorescent protein with rapid expression and cell filling properties for neuronal imaging. Proceedings of the National Academy of Sciences 117, 30710–30721. https://doi.org/10.1073/pnas.2000942117

Campbell, R.E., Tour, O., Palmer, A.E., Steinbach, P.A., Baird, G.S., Zacharias, D.A., Tsien, R.Y., 2002. A monomeric red fluorescent protein. Proceedings of the National Academy of Sciences 99, 7877–7882. https://doi.org/10.1073/pnas.082243699

Chalfie, M., Tu, Y., Euskirchen, G., Ward, W.W., Prasher, D.C., 1994. Green Fluorescent Protein as a Marker for Gene Expression. Science 263, 802–805. https://doi.org/10.1126/science.8303295

Chudakov, D.M., Matz, M.V., Lukyanov, S., Lukyanov, K.A., 2010. Fluorescent Proteins and Their Applications in Imaging Living Cells and Tissues. Physiological Reviews 90, 1103–1163. https://doi.org/10.1152/physrev.00038.2009

Cormack, B.P., Valdivia, R.H., Falkow, S., 1996. FACS-optimized mutants of the green fluorescent protein (GFP). Gene 173, 33–38. https://doi.org/10.1016/0378-1119(95)00685-0

Cranfill, P.J., Sell, B.R., Baird, M.A., Allen, J.R., Lavagnino, Z., de Gruiter, H.M., Kremers, G.-J., Davidson, M.W., Ustione, A., Piston, D.W., 2016. Quantitative assessment of fluorescent proteins. Nature Methods 13, 557–562. https://doi.org/10.1038/nmeth.3891

Ducret, A., Quardokus, E.M., Brun, Y.V., 2016. MicrobeJ, a tool for high throughput bacterial cell detection and quantitative analysis. Nature Microbiology 1, 16077. https://doi.org/10.1038/nmicrobiol.2016.77

Gadella, T.W.J., van Weeren, L., Stouthamer, J., Hink, M.A., Wolters, A.H.G., Giepmans, B.N.G., Aumonier, S., Dupuy, J., Royant, A., 2023. mScarlet3: a brilliant and fast-maturing red fluorescent protein. Nature Methods 20, 541–545. https://doi.org/10.1038/s41592-023-01809-y

Goedhart, J., von Stetten, D., Noirclerc-Savoye, M., Lelimousin, M., Joosen, L., Hink, M.A., van Weeren, L., Gadella, T.W.J., Royant, A., 2012. Structure-guided evolution of cyan fluorescent proteins towards a quantum yield of 93%. Nature Communications 3, 751. https://doi.org/10.1038/ncomms1738

Goormaghtigh, F., Fraikin, N., Putrinš, M., Hallaert, T., Hauryliuk, V., Garcia-Pino, A., Sjödin, A., Kasvandik, S., Udekwu, K., Tenson, T., Kaldalu, N., Van Melderen, L., 2018. Reassessing the Role of Type II Toxin-Antitoxin Systems in Formation of Escherichia coli Type II Persister Cells. mBio 9, e00640-18. https://doi.org/10.1128/mBio.00640-18

Govers, S.K., Mortier, J., Adam, A., Aertsen, A., 2018. Protein aggregates encode epigenetic memory of stressful encounters in individual Escherichia coli cells. PLOS Biology 16, e2003853. https://doi.org/10.1371/journal.pbio.2003853

Heim, R., Prasher, D.C., Tsien, R.Y., 1994. Wavelength mutations and posttranslational autoxidation of green fluorescent protein. Proceedings of the National Academy of Sciences 91, 12501–12504. https://doi.org/10.1073/pnas.91.26.12501

Kremers, G.-J., Goedhart, J., van Munster, E.B., Gadella, T.W.J., 2006. Cyan and Yellow Super Fluorescent Proteins with Improved Brightness, Protein Folding, and FRET Förster Radius,. Biochemistry 45, 6570–6580. https://doi.org/10.1021/bi0516273

Lambert, G.G., Depernet, H., Gotthard, G., Schultz, D.T., Navizet, I., Lambert, T., Adams, S.R., Torreblanca-Zanca, A., Chu, M., Bindels, D.S., Levesque, V., Nero Moffatt, J., Salih, A., Royant, A., Shaner, N.C., 2020. Aequorea's secrets revealed: New fluorescent proteins with unique properties for bioimaging and biosensing. PLOS Biology 18, e3000936. https://doi.org/10.1371/journal.pbio.3000936

Landgraf, D., Okumus, B., Chien, P., Baker, T.A., Paulsson, J., 2012. Segregation of molecules at cell division reveals native protein localization. Nature Methods 9, 480–482. https://doi.org/10.1038/nmeth.1955

Lee, J., Liu, Z., Suzuki, P.H., Ahrens, J.F., Lai, S., Lu, X., Guan, S., St-Pierre, F., 2020. Versatile phenotype-activated cell sorting. Science Advances 6, eabb7438. https://doi.org/10.1126/sciadv.abb7438

Matz, M.V., Fradkov, A.F., Labas, Y.A., Savitsky, A.P., Zaraisky, A.G., Markelov, M.L., Lukyanov, S.A., 1999. Fluorescent proteins from nonbioluminescent Anthozoa species. Nature Biotechnology 17, 969–973. https://doi.org/10.1038/13657

Nguyen, A.W., Daugherty, P.S., 2005. Evolutionary optimization of fluorescent proteins for intracellular FRET. Nature Biotechnology 23, 355–360. https://doi.org/10.1038/nbt1066

Ogawa, H., Inouye, S., Tsuji, F.I., Yasuda, K., Umesono, K., 1995. Localization, trafficking, and temperature-dependence of the Aequorea green fluorescent protein in cultured vertebrate cells. Proceedings of the National Academy of Sciences 92, 11899–11903. https://doi.org/10.1073/pnas.92.25.11899

Ormö, M., Cubitt, A.B., Kallio, K., Gross, L.A., Tsien, R.Y., Remington, S.J., 1996. Crystal Structure of the Aequorea victoria Green Fluorescent Protein. Science 273, 1392–1395. https://doi.org/10.1126/science.273.5280.1392

Pédelacq, J.-D., Cabantous, S., Tran, T., Terwilliger, T.C., Waldo, G.S., 2006. Engineering and characterization of a superfolder green fluorescent protein. Nature Biotechnology 24, 79–88. https://doi.org/10.1038/nbt1172

Rousseau, C.J., Fraikin, N., Zedek, S., Van Melderen, L., 2023. Are envelope stress responses essential for persistence to β-lactams in Escherichia coli? Antimicrobial Agents and Chemotherapy 67, e00329-23. https://doi.org/10.1128/aac.00329-23

Shaner, N.C., Campbell, R.E., Steinbach, P.A., Giepmans, B.N.G., Palmer, A.E., Tsien, R.Y., 2004. Improved monomeric red, orange and yellow fluorescent proteins derived from Discosoma sp. red fluorescent protein. Nature Biotechnology 22, 1567–1572. https://doi.org/10.1038/nbt1037

Shaner, N.C., Lambert, G.G., Chammas, A., Ni, Y., Cranfill, P.J., Baird, M.A., Sell, B.R., Allen, J.R., Day, R.N., Israelsson, M., Davidson, M.W., Wang, J., 2013. A bright monomeric green fluorescent protein derived from Branchiostoma lanceolatum. Nature Methods 10, 407–409. https://doi.org/10.1038/nmeth.2413

Shaner, N.C., Lin, M.Z., McKeown, M.R., Steinbach, P.A., Hazelwood, K.L., Davidson, M.W., Tsien, R.Y., 2008. Improving the photostability of bright monomeric orange and red fluorescent proteins. Nature Methods 5, 545–551. https://doi.org/10.1038/nmeth.1209

Teerawanichpan, P., Hoffman, T., Ashe, P., Datla, R., Selvaraj, G., 2007. Investigations of combinations of mutations in the jellyfish green fluorescent protein (GFP) that afford brighter fluorescence, and use of a version (VisGreen) in plant, bacterial, and animal cells. Biochimica et Biophysica Acta (BBA) - General Subjects 1770, 1360–1368. https://doi.org/10.1016/j.bbagen.2007.06.005

Valbuena, F.M., Fitzgerald, I., Strack, R.L., Andruska, N., Smith, L., Glick, B.S., 2020. A photostable monomeric superfolder green fluorescent protein. Traffic 21, 534–544. https://doi.org/10.1111/tra.12737

Yoshioka-Kobayashi, K., Matsumiya, M., Niino, Y., Isomura, A., Kori, H., Miyawaki, A., Kageyama, R., 2020. Coupling delay controls synchronized oscillation in the segmentation clock. Nature 580, 119–123. https://doi.org/10.1038/s41586-019-1882-z

Zacharias, D.A., Violin, J.D., Newton, A.C., Tsien, R.Y., 2002. Partitioning of Lipid-Modified Monomeric GFPs into Membrane Microdomains of Live Cells. Science 296, 913–916. https://doi.org/10.1126/science.1068539

Zaslaver, A., Bren, A., Ronen, M., Itzkovitz, S., Kikoin, I., Shavit, S., Liebermeister, W., Surette, M.G., Alon, U., 2006. A comprehensive library of fluorescent transcriptional reporters for Escherichia coli. Nature Methods 3, 623–628. https://doi.org/10.1038/nmeth895

Zhang, G., Gurtu, V., Kain, S.R., 1996. An Enhanced Green Fluorescent Protein Allows Sensitive Detection of Gene Transfer in Mammalian Cells. Biochemical and Biophysical Research Communications 227, 707–711. https://doi.org/10.1006/bbrc.1996.1573